Metastable states during magnetization reversal in square permalloy rings

P. Vavassori,[1] M. Grimsditch,[2] V. Novosad,[2] V. Metlushko,[3] and B. Ilic[4]
[1]*INFM UdR of Ferrara–Dipartimento di Fisica, Università di Ferrara, I-44100 Ferrara, Italy and INFM–National Research Center on Nanostructures and Biosystems at Surfaces, I-44100 Ferrara, Italy*
[2]*Materials Science Division, Argonne National Laboratory, Argonne, Illinois 60439*
[3]*Department of Electrical and Computer Engineering, University of Illinois at Chicago, Chicago, Illinois 60607*
[4]*Cornell Nanofabrication Facility, Cornell University, Ithaca, New York 14853*
(Received 12 November 2002; revised manuscript received 12 February 2003; published 28 April 2003)

The magnetic reversal process in a two-dimensional array of permalloy square rings is presented. Rings of thickness of 25 nm, of lateral size of 2.1 μm, and with ring width of 240 nm were microfabricated using electron-beam lithography and lift-off techniques. Analysis of the diffracted magneto-optical Kerr effect hysteresis loops, magnetic force microscopy images, and micromagnetic simulations show that the magnetization reversal path depends on the direction of the in-plane applied magnetic field. On reducing the field from saturation, for fields along an edge or a diagonal of the square, the ''onion'' state is the stable state at remanence. In a narrow field range around reversal we find that the reversal occurs via a metastable intermediate state. For fields along the diagonal this intermediate state is a magnetic vortex. When the field is applied along an edge direction the intermediate state is a ''horseshoe'' state.

DOI: 10.1103/PhysRevB.67.134429 PACS number(s): 75.75.+a, 75.60.Jk, 78.20.Ls

INTRODUCTION

The size and shape control offered by state-of-the-art lithography techniques has made it possible to investigate material properties at length scales previously unattainable. One area of intense activity is the study of magnetism at the nanometer length scale.[1–10] For particles of this size, because intrinsic magnetic length scales are comparable to the sample dimensions, novel physical properties can be expected. This field has attracted much attention because of its close ties to potential technological applications. In this connection, a key issue in fundamental physics and data storage technology is to understand and control the magnetic switching of small magnetic elements. Because of the large dipolar demagnetizing fields close to the element's borders, the magnetic equilibrium configurations and switching mechanisms are sensitive to subtle shape variations and to edge roughness. In elements developing a vortex state these effects play a lesser role due to the magnetic flux closure, which makes this magnetic configuration very stable.[11,12] The stability of the vortex state can be considerably improved if the highly energetic vortex core is removed by using a ring element.[13] Because of their reduced sensitivity to edge defects, ring magnets have been proposed for use in magnetic random access memories.[14,15]

Concomitant with the development of fabrication techniques, characterization techniques for submicron samples have also undergone notable improvements. Many techniques are now available to investigate the structure and response of nanosized magnetic particles. Typically a battery of techniques is required to provide a complete picture of the magnetic behavior.

In this investigation we have used the diffracted magneto-optic Kerr effect[16,17] (D-MOKE) to obtain information on the magnetization reversal in arrays of square permalloy rings. This technique provides information about the magnetic configurations that develop during switching inside each element of an array. Interestingly, the spatial resolution obtainable with this technique can be smaller than the wavelength of the laser light used for the measurements. The ability of diffracted MOKE to achieve this is a combination of both the wavelength of the radiation and the magnetic form factors of particles that are themselves comparable to the wavelength.

Our experimental D-MOKE loops are compared with loops extracted from micromagnetic simulations, using the theoretical approach reported in Ref. 18. With some assumptions regarding the ring shape the simulations reproduce the experimental D-MOKE loops and show a two-step reversal mechanism in which either a vortex or a ''horseshoe'' metastable intermediate state is generated, depending on the direction of the applied field. By suitably choosing the field history it has been possible to ''quench'' these metastable states to zero applied field and to observe them using magnetic force microscopy (MFM).

Experimental details

The array of square rings was fabricated by a combination of electron-beam lithography and lift-off techniques. To begin with, a standard silicon wafer is spin-coated with a positive-type poly(methyl methacrylate) (PMMA) resist. The sample was then patterned using a modified JEOL 840 scanning electron microscope (SEM) equipped with a Raith pattern generating software,[19] an electron-beam current of 100 pA, and an accelerating voltage of 35 keV. The magnetic film is deposited on the water-cooled substrate from an $Fe_{19}Ni_{81}$ (permalloy) target using an electron-beam evaporator in a vacuum of about 10^{-7} Pa. The as-deposited reference film is magnetically soft with coercive and uniaxial anisotropy fields of a few oersteds. Finally, after ultrasonic-assisted lift-off, arrays of permalloy square rings of thickness 25 nm, lateral size 2.1 μm, and 240 nm ring width, arranged on a 4 μm square lattice, are obtained. The array used for our experiments is shown in Fig. 1.

The experimental D-MOKE setup and the magnetic form factor formalism used for the interpretation of the measured

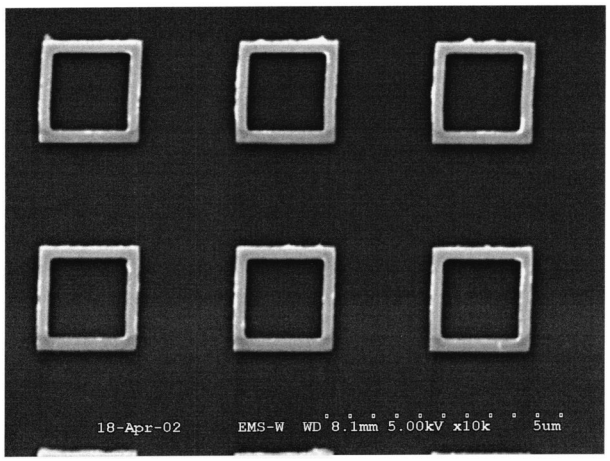

FIG. 1. SEM image of square permalloy rings.

loops have been described in Refs. 7 and 18. The magnetic form factors of order n (f_n) are defined by

$$f_n = \int m \exp(in\mathbf{G}\cdot\mathbf{r})dS, \tag{1}$$

where m is the magnetization component appropriate for the experimental Kerr geometry (i.e., perpendicular to the scattering plane for our transverse MOKE geometry), **G** is a reciprocal-lattice vector, n is an integer, and the integral is carried out over a ring. It is clear, therefore, that the form factors contain information about the magnetization distribution within a unit cell.

The intensity (I) of the measured loops has been shown[7,18] to be proportional to

$$I = \mathrm{Re}[f_n] + A_n\,\mathrm{Im}[f_n], \tag{2}$$

where A_n is a number that depends on the diffraction order. The value of A_n can be calculated via the Stratton-Silver-Chu integral using the physical-optics approximation.[20] Using the refractive index values of permalloy and silicon[21,22] and the permalloy magneto-optic coupling constant,[21] we obtain (for the 45° incidence angle geometry adopted in our measurements) values of A_n shown in Fig. 2. The absolute values of A_n, however, turn out to be very sensitive to the numerical parameters used in the calculation. Using other sets of material parameters reported in literature and/or changes in dot thickness, we obtain similarly shaped curves but with different offsets along the y axis. For some combination of values even the sign of A can change as the diffraction order is varied. Because of the uncertainty in determining A, for our simulated loops, we have we chosen the value of $A_1 = -1.3$ that best accounts for the measured first-order loop. The other A_n were deduced from the suitably shifted curve (dashed line in Fig. 2); all lie in the range -1.2 to -1.3.

The magnetic form factors are evaluated via Eq. (1) and the magnetization profile calculated using the micromagnetic OOMMF code[23] at each field. Once the form factors are known the magneto-optical loops of any given order (n) can be obtained from Eq. (2).

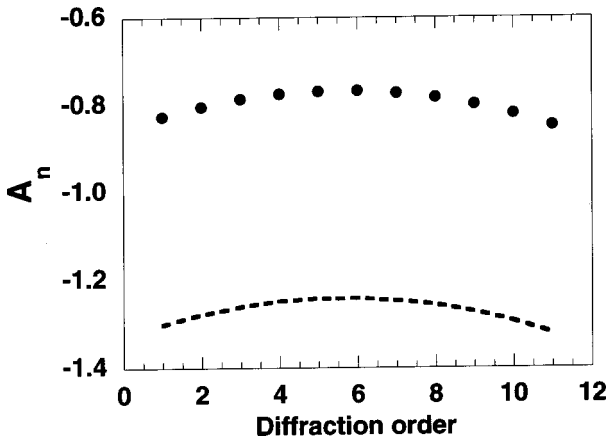

FIG. 2. Plot of the relative contribution of the imaginary and real parts of the magnetic form factor for different diffraction orders. The symbols are calculated as described in the text. Because of uncertainties in the material parameters we have rescaled the calculated values (dashed line) to produce agreement with the first order experimental diffraction loop.

The array of permalloy squares was investigated by MFM in a Dimension™ 3000 scanning probe microscope from Digital Instruments (DI).[24] Topographic and magnetic images were obtained with the instrument operated in the tapping LiftMode™ using the standard CoCr-coated MFM tips from DI. Typical scan heights were about 70 nm.

RESULTS

Diffracted MOKE

D-MOKE hysteresis loops, measured for two directions of the applied field (H), are shown in Fig. 3 (H along the ring edge) and Fig. 4 (H along the ring diagonal). There are two reasons why fewer loops are shown for the second case: The reciprocal-lattice vector for the diagonal case is $\sqrt{2}$ larger, and hence $\sqrt{2}$ less diffraction spots are observed. The diffracted spots are also much weaker for the diagonal case as can be ascertained by calculating the nonmagnetic form factor. To facilitate comparison the corresponding calculated loops, which will be presented and discussed later, are introduced here as Figs. 5 and 6. The zero order loops in Figs. 3 and 4 can be understood based on simple arguments schematically shown in Fig. 7: At high fields all four sides of the ring are aligned along the field direction (states 1 in Fig. 7). As the field is reduced, shape anisotropy aligns the magnetization parallel to each branch of the ring and leads, at remanence, to the onion states (schematic 2 in Fig. 7). We note that the left-right asymmetry in the upper 2 and 4 states results from the assumption that the applied field will never be ''perfectly'' aligned along an edge direction. In the onion state the magnetization for H parallel to an edge and along the diagonal is reduced to 1/2 and $1/\sqrt{2}$ of the saturation value, respectively.

As H is reduced further (i.e., to negative values) by symmetry one might expect both branches of the onion states described above to reverse simultaneously, leading directly to state 4. Micromagnetic simulations of a perfect ring struc-

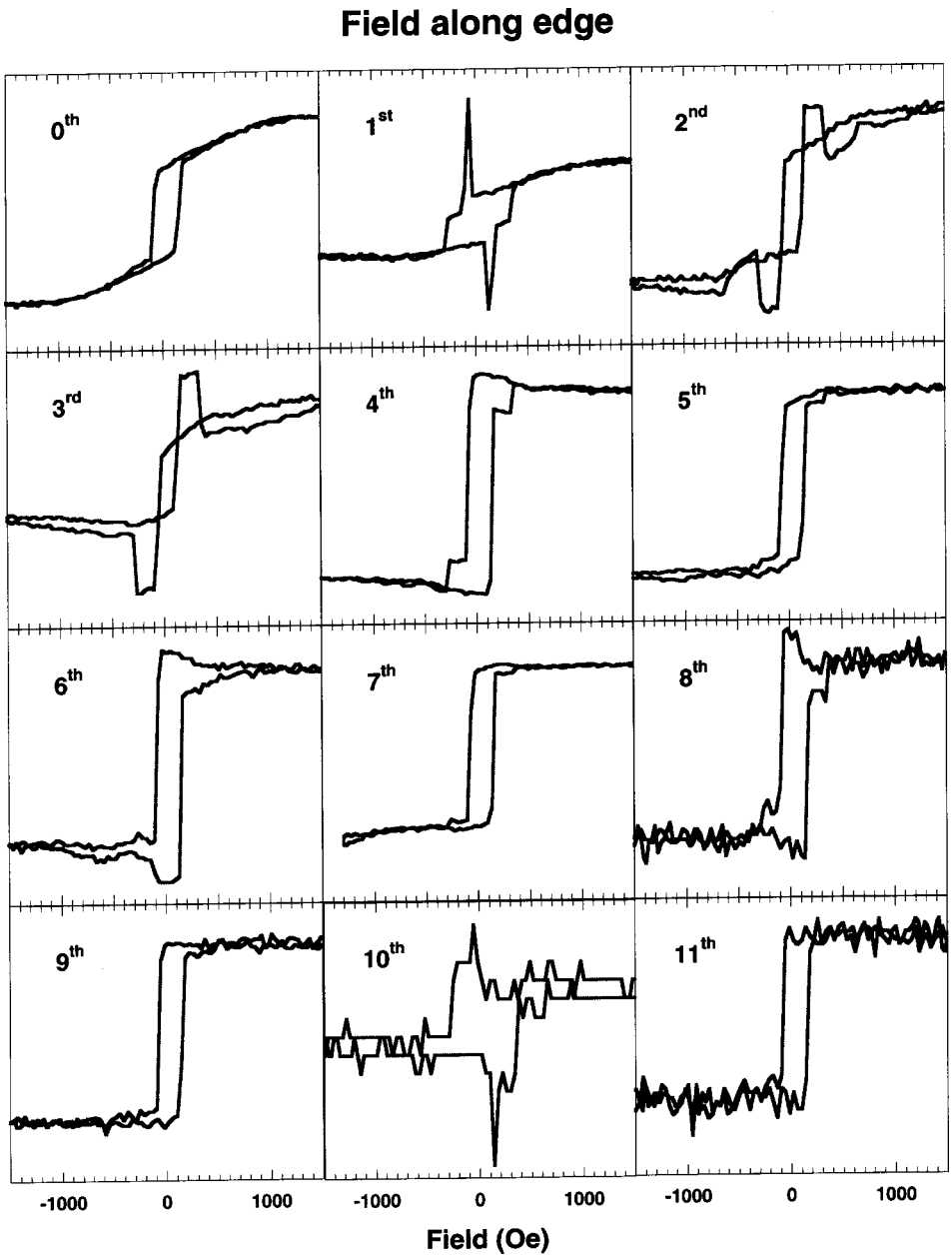

FIG. 3. Experimental D-MOKE loops for H parallel to the edge of the squares.

ture (see below) confirm this expectation but they fail to reproduce the rich structure in the higher-order D-MOKE loops.

Furthermore, many of the higher-order loops show some evidence for structure in the narrow field interval close to switching. In particular the first-order loops, for both directions of the field, show a very strong feature at the switching field. Since these features contain information about the most significant jump of the reversal, they warrant more detailed attention.

Micromagnetic simulations

Micromagnetic simulations have been performed on the reversal in a single (perfect) square ring (2.1 μm per side and 240 nm wide branches). We used 210×210 calculation cells (for a total of 44 100 computational cubic cells each one with a side of 10 nm). The material parameters used for the simulation are[24] a saturation magnetization of 660×10^3 A/m and an exchange constant of 13×10^{-12} J/m. It has been shown[25,26] that the size of the micromagnetic cells must be made 6–7 times larger than the exchange length (≈5 nm). Although we are certainly in this limit, we have verified, in one instance, that a simulation with 7.5 nm cells produces no significant change. The field in the simulations is applied at 2° from the edge and diagonal directions in order to simulate the experiments where perfect alignment is unlikely to be achieved. All the form factors extracted from the simulation of perfect rings have zero imaginary parts. The resulting hysteresis loops, although they reproduce the zeroth-order loops, do not yield any structure in the higher order loops and most notably do not reproduce the strong peaks observed in the

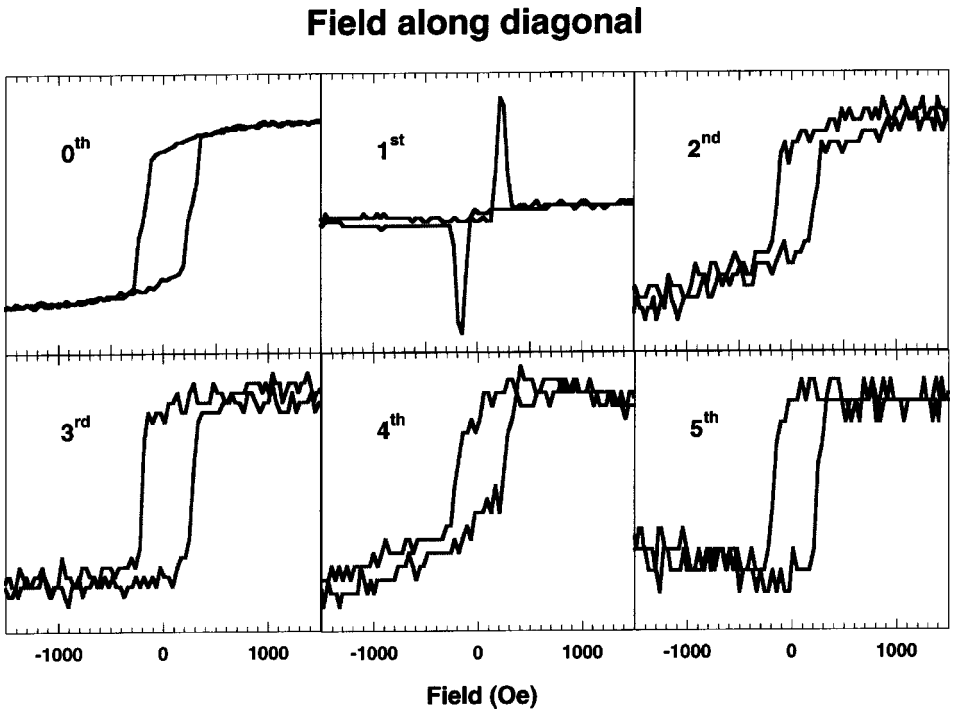

FIG. 4. Experimental D-MOKE loops for H along the diagonal.

first-order experimental loops. These simulations predict an abrupt reversal from one onion state to its mirror state (state 2 to state 4 in Fig. 7).

From Eq. (1) we have

$$\mathrm{Re}[f_1^m] = \int m_y \cos[\mathbf{G}\cdot\mathbf{r}]\,dS$$

and

$$\mathrm{Im}[f_1^m] = \int m_y \sin[\mathbf{G}\cdot\mathbf{r}]\,dS,$$

and the integral is carried out over $-d/2 < |\mathbf{r}| < d/2$. For H along an edge we have $|\mathbf{G}| = 2\pi/d$ (d is the lattice spacing) and, since the ring size is equal to $d/2$, we see that $\mathrm{Re}[f_1^m]$ and $\mathrm{Im}[f_1^m]$ are weighted towards the magnetization in the horizontal and vertical branches, respectively. Since the horizontal branches rotate monotonically, the resulting $\mathrm{Re}[f_1^m]$ is expected to be a smoothly varying function of field. $\mathrm{Im}[f_1^m]$, on the other hand, will be zero if the ring maintains a left-right symmetry in m_y and can become large only if this

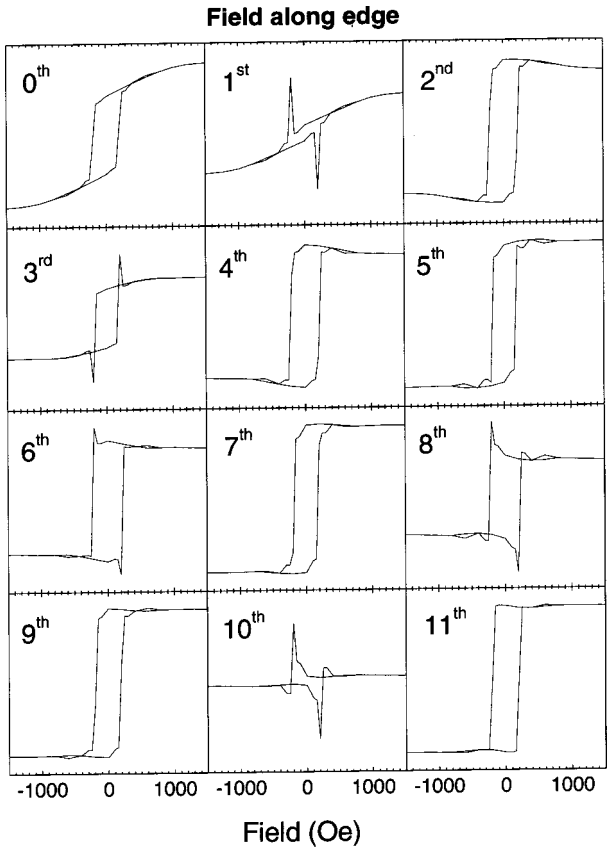

FIG. 5. Calculated D-MOKE loops for H parallel to the edge of the squares.

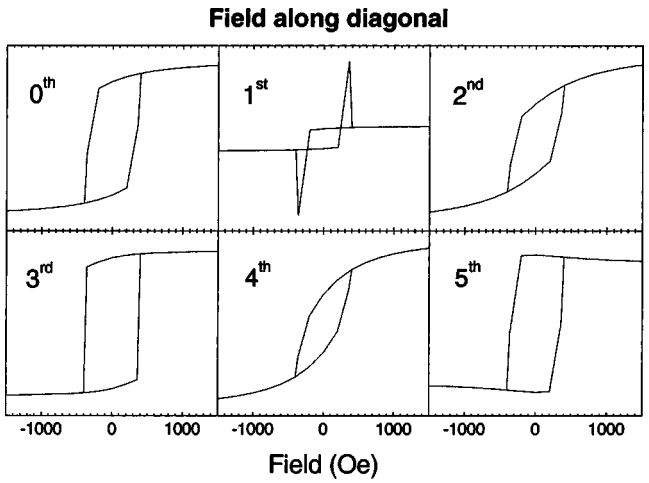

FIG. 6. Calculated D-MOKE loops for H along the diagonal.

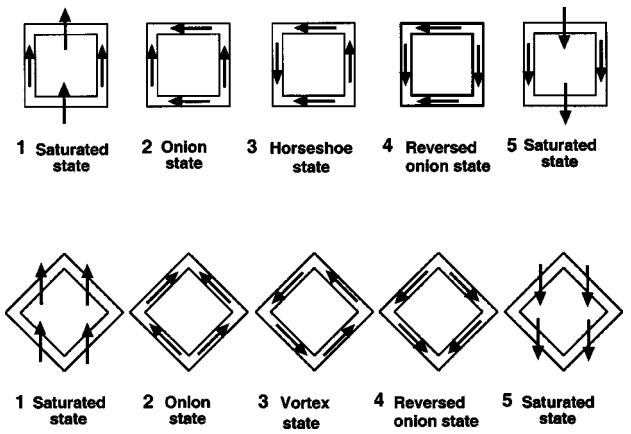

FIG. 7. Schematic of magnetic states generated during reversal.

symmetry is broken during the reversal.[18] Based on the simple arguments above, we would expect strong contributions from the imaginary part only if an asymmetric (i.e., nonsimultaneous) switching took place in the vertical branches.

As was shown in Ref. 13 by introducing an asymmetry between the two lateral branches of the ring (we made the left and right branches of the ring 22 and 24 cells wide) the micromagnetic simulations show a nonsimultaneous reversal of the lateral branches. This effect has also been observed experimentally in Ref. 27. The resulting calculated loops, shown in Figs. 5 and 6, produce excellent agreement with the experimental loops in Figs. 3 and 4. In particular they reproduce the sharp spikes present in the first-order loops. Analysis of the micromagnetic simulation structures that develop during reversal confirm the presence of states 1, 2, 4, and 5 in Fig. 7 that were postulated above based on simple energy considerations. Additionally, however, they show that between states 2 and 4 the rings transform to an intermediate state. For H along the diagonal it predicts reversal via an intermediate vortex state (state 3 in the lower part of Fig. 7) rather than from one onion state to its mirror state. For H along the ring edge the simulations predict configuration 3 in the upper part of Fig. 7 which we call the horseshoe state.

Although the micromagnetically generated loops in Figs. 6 and 7 reproduce most of the salient features of the experimental loops in Figs. 3 and 4 (note for example the spikes in the tenth-order loops in Figs. 3 and 5), some of the features are not reproduced. Most notable perhaps are the differences between the second-order loops in Figs. 3 and 5. Many of the experimental loops show some indication that the reversal might include an additional metastable step. At present we are unable to conceive of any additional process (e.g., anisotropy, distribution of ring properties, thickness inhomogeneities, etc.) that might lead to such a mechanism. Any future micromagnetic simulations that achieve an improved description of the experimental loops, especially the second-order loop in Fig. 3, will also, however, be required to yield correct descriptions of all the loops in Fig. 3.

MFM

Confirmation of the existence of the metastable vortex and horseshoe states was obtained using MFM techniques.

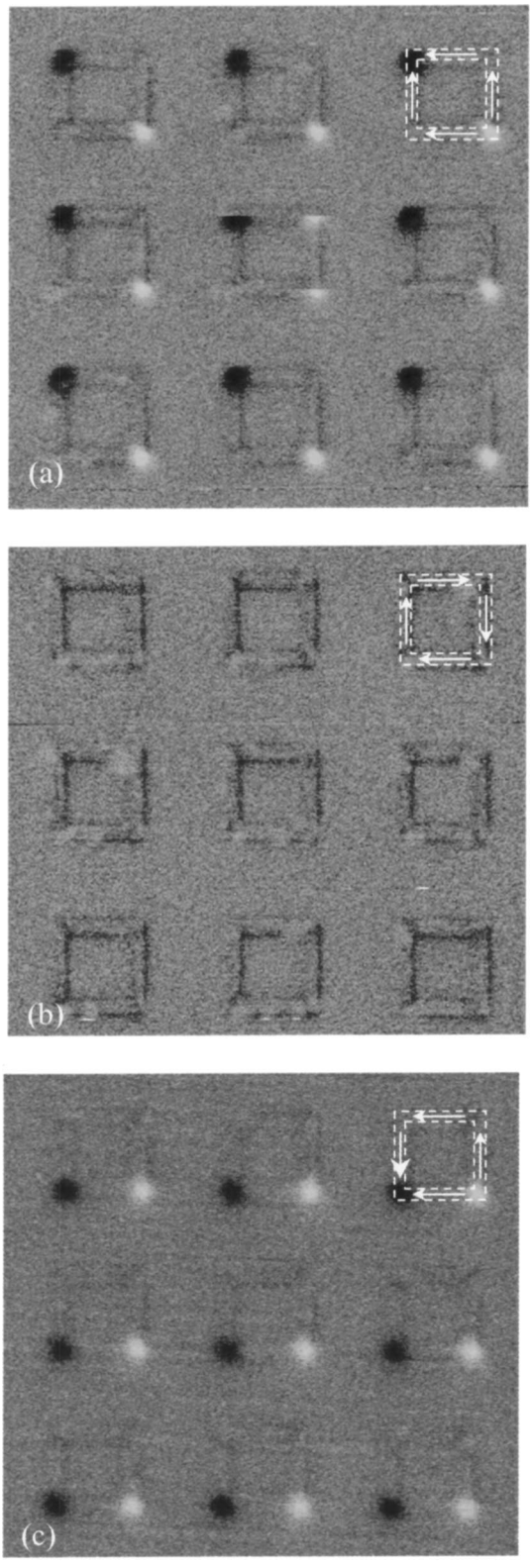

FIG. 8. MFM images of (a) an onion state, (b) a vortex state, and (c) a horseshoe state in square rings. The dashed outline of the top, right ring in each image has been transferred from the corresponding AFM image and the direction of magnetization, inferred from the MFM image, is indicated by arrows.

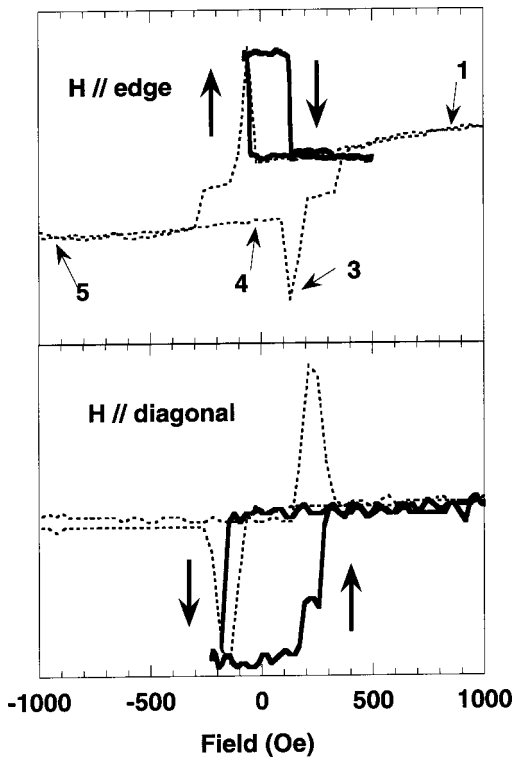

FIG. 9. Asymmetric first-order D-MOKE loops for *H* along an edge (upper) and a diagonal (lower). The symmetric loops, taken from Figs. 3 and 4, are indicated by the dashed lines. The numbers in the upper plot indicate the magnetic state sketched in Fig. 7.

The signal in MFM images is proportional to the second derivative of the perpendicular component of the magnetic flux density. Intense features are therefore present in MFM images whenever magnetic-flux closure is not achieved leading to characteristic images for the horseshoe, onion, and vortex states that are easily distinguishable. The onion state (obtained by simply reducing the field from saturation to zero) is shown in Fig. 8(a). Note that eight out of the nine rings are in the onion state; the center ring, with two bright spots, is most likely due to interaction with the MFM tip.

Since the intermediate vortex and horseshoe states are created at small negative fields and require an even more negative field for annihilation, it is reasonable to assume that they should be stable (or at least metastable) at zero field. It should, therefore, be possible to trap them and bring them to zero field with a suitable field history. Since these states are most clearly discernible in the first-order loops, we acquired asymmetric hysteresis loops. For *H* along an edge, when $H_{\min}=-75\pm5$ Oe we obtain loops like the one shown (full line) in the upper part of Fig. 9; also shown in this figure (dashed line) is the full first-order loop from Fig. 3. These loops show that it is possible to trap the rings in the state corresponding to the peak in the first-order loop and that this state is stable at zero field. The lower part of Fig. 9 shows the corresponding loops when *H* is along the diagonal.

Samples prepared in the above manner were subsequently measured using MFM. The resulting images are shown in Fig. 8. Figure 8(b) shows the vortex state with its characteristic low contrast. Figure 8(c) exhibits the horseshoe state proposed in Fig. 7. We note here that the horseshoe state is very unstable and can easily be erased by the MFM tip. For this reason the scan direction in Fig. 8(c) was chosen from top to bottom (horizontal rastering). Scans from bottom to top transformed about half of the horseshoe states into onion or other states.

CONCLUSIONS

The magnetic configurations that appear in square rings during reversal have been investigated with D-MOKE, micromagnetic simulations, and MFM imaging. The ring asymmetry, necessary to produce agreement between simulations and experiments, was extracted from the first-order D-MOKE loops. The ring asymmetry leads to the existence of metastable intermediate vortex or horseshoe states that that are generated between the onion and reversed onion states. By suitably choosing the field history, the vortex and horseshoe states can be quenched to zero field and imaged using MFM.

ACKNOWLEDGMENTS

Work at ANL was supported by U.S. Department of Energy, BES Materials Sciences under Contract No. W-31-109-ENG-38. P.V. gratefully acknowledges financial support from INFM, under the ''MAGDOT'' PAIS research program as well as from MURST-COFIN 2000. V.M. was supported by the U.S. NSF Grant No. ECS-0202780.

[1] S. Y. Chou, M. Wei, P. R. Krauss, and P. B. Fisher, J. Vac. Sci. Technol. B **12**, 3695 (1994).
[2] Y. Otani, S. G. Kim, T. Kohda, and K. Fukamichi, IEEE Trans. Magn. **34**, 1090 (1998).
[3] R. P. Cowburn, A. O. Adeyeye, and M. E. Welland, Phys. Rev. Lett. **81**, 5414 (1998).
[4] N. Dao, S. R. Homer, and S. L. Whittenburg, J. Appl. Phys. **86**, 3262 (1999).
[5] R. D. Gomez, T. V. Luu, A. O. Pak, K. J. Kirk, and J. N. Chapman, J. Appl. Phys. **85**, 6163 (1999).
[6] J. Yu, U. Rüdiger, L. Thomas, S. S. P. Parkin, and A. D. Kent, J. Appl. Phys. **85**, 5501 (1999).
[7] I. Guedes, M. Grimsditch, V. Metlushko, P. Vavassori, B. Ilic, P. Neuzil, and R. Kumar, Phys. Rev. B **66**, 014434 (2002).
[8] R. P. Cowburn, D. K. Koltsov, A. O. Adeyeye, M. E. Welland, and D. M. Tricker, Phys. Rev. Lett. **83**, 1042 (1999).
[9] J. Johnson, M. Grimsditch, V. Metlushko, P. Vavassori, B. Ilic, P. Neuzil, and R. Kumar, Appl. Phys. Lett. **77**, 4410 (2000).
[10] A. Lebib, S. P. Li, M. Natali, and Y. Chen, J. Appl. Phys. **89**, 3892 (2001).
[11] T. Shinjo, T. Okuno, R. Hassdorf, K. Shigeto, and T. Ono, Science **289**, 930 (2000).
[12] S. P. Li, D. Peyrade, M. Natali, A. Lebib, Y. Chen, U. Ebels, L. D. Buda, and K. Ounadjela, Science **289**, 1102 (2001).

[13] J. Rothman, M. Kläui, L. Lopez-Diaz, C. A. F. Vaz, A. Bleloch, J. A. C. Bland, Z. Cui, and R. Speaks, Phys. Rev. Lett. **86**, 1098 (2001).
[14] Jian-Gang Zhu, Youfeng Zheng, and Gary A. Prinz, J. Appl. Phys. **87**, 6668 (2000).
[15] M. Kläui, C. A. F. Vaz, J. A. C. Bland, W. Wernsdorfer, G. Faini, and E. Cambril, Appl. Phys. Lett. **81**, 108 (2002).
[16] O. Geoffroy, D. Givord, Y. Otani, B. Pannetier, A. D. dos Santos, M. Schlenker, and Y. Souche, J. Magn. Magn. Mater. **121**, 516 (1993).
[17] P. Vavassori, V. Metlushko, R. Osgood III, M. Grimsditch, U. Welp, G. Crabtree, Wenjun Fan, S. Brueck, B. Ilic, and P. Hesketh, Phys. Rev. B **59**, 6337 (1999).
[18] M. Grimsditch, P. Vavassori, V. Novosad, V. Metlushko, H. Shima, Y. Otani, and K. Fukamichi, Phys. Rev. B **65**, 172419 (2002).
[19] Raith Elphy quantum universal SEM nanolithography system, Version 2.07, April 2001, Germany.
[20] R. M. A. Azzam and N. M. Bashara, Phys. Rev. B **5**, 4721 (1972).
[21] A. Berger and M. R. Pufall, Appl. Phys. Lett. **71**, 965 (1997).
[22] D. E. Aspnes and A. A. Studna, Phys. Rev. B **27**, 985 (1983).
[23] M. J. Donahue and D. J. Porter, User's Guide OOMMF Version 1.0 (National Institute of Standards and Technology, Gaithersburg, MD, 1999).
[24] Digital Instruments (www.di.com).
[25] M. E. Schabes and N. Bertram, J. Appl. Phys. **64**, 1347 (1988).
[26] W. Rave, K. Fabian, and A. Hubert, J. Magn. Magn. Mater. **190**, 332 (1998).
[27] M. Kläui, J. Rothman, L. Lopez-Dias, C. A. F. Vaz, J. A. C. Bland, and Z. Cui, Appl. Phys. Lett. **78**, 3268 (2001).